

SuperMat: Physically Consistent PBR Material Estimation at Interactive Rates

Yijia Hong¹, Yuan-Chen Guo², Ran Yi¹, Yulong Chen¹, Yan-Pei Cao², Lizhuang Ma¹
¹Shanghai Jiao Tong University, ²VAST



Figure 1. We present an efficient method for high-quality material decomposition in both 2D and 3D. **Left:** Albedo and RM predictions of SuperMat on rendered images under unknown illumination. The first row shows inputs with uneven lighting, the second row displays albedo predictions, and the third row presents RM predictions. **Middle:** Rendering results of a 3D object with PBR materials obtained by our method under novel lighting. **Right:** Our method is efficient and produces high-quality results.

Abstract

Decomposing physically-based materials from images into their constituent properties remains challenging, particularly when maintaining both computational efficiency and physical consistency. While recent diffusion-based approaches have shown promise, they face substantial computational overhead due to multiple denoising steps and separate models for different material properties. We present SuperMat, a single-step framework that achieves high-quality material decomposition with one-step inference. This enables end-to-end training with perceptual and re-render losses while decomposing albedo, metallic, and roughness maps at millisecond-scale speeds. We further extend our framework to 3D objects through a UV refinement network, enabling consistent material estimation across viewpoints while maintaining efficiency. Experiments demonstrate that SuperMat achieves state-of-the-art PBR material decomposition quality while reducing inference time from seconds to

milliseconds per image, and completes PBR material estimation for 3D objects in approximately 3 seconds.

1. Introduction

Decomposing physically-based materials from images into their constituent properties (e.g., albedo, metallic, and roughness maps) remains a central challenge in computer vision and graphics. This task is essential for creating high-fidelity 3D assets across numerous applications, from film production and game development to virtual and augmented reality pipelines. While recent advances have shown promising results [5, 23, 41], the problem remains challenging due to its ill-posed nature, particularly given unknown lighting conditions and complex interactions between different material properties. Our work addresses two key objectives: **1)** efficient decomposition of high-fidelity material maps from 2D images, and **2)** extension of this capability to 3D objects, enabling accurate material estimation

across complex geometries.

Previous works in this domain generally fall into two main categories: optimization-based and data-driven approaches. 1) Optimization-based methods [2, 6, 11, 14–16, 21, 27, 42–44] employ differentiable rendering and neural representations to reconstruct 3D objects with material parameters by minimizing the difference between rendered and target images. While these methods achieve reasonable view consistency, they often compromise material quality, producing artifacts such as blurred boundaries and physically implausible parameters, particularly in metallic and roughness properties. 2) Data-driven approaches [20, 36, 47], particularly recent ones [5, 23, 41], leverage large diffusion models and reframe material decomposition as a conditional image generation task. However, these methods tend to focus solely on individual material properties, overlooking the interactions between different types of materials and combined impact on rendered appearances. Even minor inaccuracies in individual material estimates can propagate through the rendering pipeline, leading to substantial visual artifacts. Moreover, current methods face considerable computational overhead - optimization-based approaches require costly geometric optimization, while diffusion-based methods demand multiple denoising steps (30-50) during inference, causing a critical bottleneck for real-time applications.

To address these challenges, we propose a deterministic one-step framework that achieves both efficient and high-quality material decomposition. First, inspired by HyperHuman [24], we introduce structural expert branches within the UNet architecture. These specialized branches enable concurrent processing of multiple material properties while maintaining domain-specific expertise, allowing our model to decompose albedo, metallic, and roughness maps simultaneously with minimal computational overhead. This design significantly improves consistency between different material properties while avoiding the linear cost scaling typically required when estimating multiple material attributes. Second, we address the computational inefficiency of traditional diffusion models by reformulating the DDIM sampling process [12, 37]. Through careful analysis and modification of the scheduler, we achieve single-step inference without compromising quality, dramatically reducing inference time. Most importantly, this single-step formulation enables end-to-end training of the diffusion model, allowing us to compute the perceptual and re-render loss on final predicted material textures, which enhances shadow removal and improves the joint performance of decomposed materials under varying lighting conditions. These advances culminate in *SuperMat*, a highly efficient image space material decomposition model that estimates high-fidelity albedo, metallic, and roughness maps at *millisecond-scale speeds*.

For practical 3D applications, we further extend SuperMat’s capabilities to handle 3D objects. We design a UV refinement network that processes SuperMat’s per-view predictions in UV space, addressing the challenge of maintaining consistency across different viewpoints while preserving the efficiency of our 2D approach. Integrated with SuperMat, this pipeline processes a textured 3D model in approximately *3 seconds*, producing high-quality material maps that maintain consistency across arbitrary viewpoints and lighting conditions.

In summary, our contributions are:

- We propose SuperMat, a novel image space material decomposition model that generates physically consistent albedo, metallic, and roughness maps simultaneously with a single-step inference process. Our method achieves state-of-the-art performance on diverse datasets, significantly outperforming previous diffusion-based works in speed.
- With the help of structural expert branches and single-step inference, we successfully achieve end-to-end training with perceptual loss and re-render loss on diffusion models in the material decomposition process, significantly enhancing both material prediction quality and rendering fidelity.
- We propose an efficient PBR material decomposition method for 3D models. Combining SuperMat and our UV refinement network, this pipeline generates high-quality PBR materials for 3D objects from baked textures in approximately 3 seconds.

2. Related Works

Material Decomposition. Recognizing the importance of material information in 3D assets, researchers have increasingly focused on material decomposition for objects and scenes. Several inverse rendering approaches [6, 14, 42] aim to reconstruct material-rich 3D representations from single or multi-view images under fixed lighting models. Although assumptions involving extra constraints can simplify the problem and yield valuable insights, they also limit the practical applicability of these methods. Other works [2, 11, 15, 16, 21, 27, 43, 44] focus on estimating both material properties and unknown illumination. As available information decreases, researchers have found that in addition to inverse control over material generation through rendered results, directly acquiring image space material priors is feasible. This shift has inspired a new wave of material decomposition methods [5, 20, 23, 25, 36, 39, 41, 47] targeting 2D images captured or rendered under unknown lighting conditions. However, challenges remain, as limitations in training data, network architecture, and training methods continue to leave room for substantial improvements in decomposition quality.

Diffusion Models. Recently, researchers have applied dif-

fusion models to a range of tasks [4, 29, 30, 35, 45], demonstrating the effectiveness of casting outcome prediction as a conditional image generation process. By leveraging prior knowledge from large pre-trained models, recent studies [5, 9, 10, 13, 18, 23, 34, 38, 46] have achieved performance improvements over previous methods in tasks like depth, normal, and material estimation. However, incorporating large models introduces efficiency challenges, particularly high memory requirements and the time-intensive, multi-step denoising process needed for inference. Inspired by insights from recent work [12, 22, 24], our approach addresses these issues by significantly reducing memory and inference time, improving the feasibility of applying these models in real-world applications.

Generation in UV Space. UV maps are advantageous for fully encapsulating the appearance information of 3D models, leading several works to explore 3D object manipulation directly within the UV space. By representing the texture of an object as a learnable image, these methods [3, 32, 40] enable texture generation, inpainting, and editing, providing new avenues for 3D tasks and allowing 2D image-space techniques and insights to be applied to 3D appearances. Building on this approach, recent methods [1, 26] have applied diffusion models to refine UV maps with promising results. In this spirit, to extend SuperMat’s capability to 3D, we fine-tune a UV-space refinement diffusion model specifically.

3. Method

In this paper, we propose **SuperMat**, a image space material decomposition model fine-tuned from Stable Diffusion that efficiently generates high-quality albedo, metallic, and roughness maps simultaneously. Given a rendered or captured image of an object under an unknown lighting condition from a specific viewpoint, SuperMat generates the corresponding material maps for the model from that same viewpoint. As shown in Figure 2, SuperMat is a 2D image-to-image one-step model with **structural expert branches** that simultaneously generates both albedo and RM (Roughness, Metallic) maps, supporting **single-step inference**. Compared to previous diffusion-based methods, this model produces superior results in less time and with reduced memory usage. Our single-step formulation allows direct generation of material maps during training, in contrast to prior diffusion methods that predict noise (ϵ) or velocity (v) terms. This enables **end-to-end** optimization with both perceptual loss on the generated maps and **re-render loss** from novel lighting conditions, leading to improved material quality and rendering fidelity.

While SuperMat achieves efficient single-image material decomposition, extending this capability to 3D objects presents additional challenges. Instead of relying on optimization-based approaches like score distillation sam-

pling (SDS) that are computationally intensive and prone to mode collapse, we propose an efficient two-stage pipeline for material estimation on 3D objects. Given a 3D model with only RGB texture, we first apply SuperMat to decompose materials from multiple viewpoints. We then introduce a UV refinement network that consolidates these view-dependent predictions into complete, high-quality UV texture maps through single-step inference. As shown in Figure 3, this pipeline enables PBR material estimation for 3D objects in approximately 3 seconds per model.

Next, we first introduce the rendering model we use, followed by a detailed description of all the key components.

3.1. Physically Based Rendering (PBR) Model

We use the Cook-Torrance Bidirectional Reflectance Distribution Function (BRDF) [7] based on microfacet theory to define the materials and establish the rendering model. Following [4], for a point with coordinates $p \in \mathbb{R}^3$, albedo $a \in \mathbb{R}^3$, metallic $m \in \mathbb{R}$, roughness $r \in \mathbb{R}$, and normal variation $n \in \mathbb{R}^3$, the PBR result L observed from viewpoint $c \in \mathbb{R}^3$ is given by:

$$L(p, \omega) = a(1 - m) \int_{\Omega} L_i(p, \omega_i)(\omega_i \cdot n) d\omega_i + \int_{\Omega} \frac{DFG}{4(\omega \cdot n)(\omega_i, n)} L_i(p, \omega_i)(\omega_i \cdot n) d\omega_i, \quad (1)$$

where ω represents the direction of the outgoing light from point p to c , *i.e.*, the viewing direction. L_i denotes the incident light from the direction ω_i , and $\Omega = \{\omega_i : \omega_i \cdot n \geq 0\}$ represents the hemisphere of normals. D , F , and G are the distribution, Fresnel, and geometry functions, respectively. For the integral part, the time complexity of Monte Carlo methods is unacceptable. Given that we use ambient lighting as the light source, we compute it efficiently using the split-sum method [27].

3.2. SuperMat - Image Space Material Decomposition

Previous works [5, 23, 41] have demonstrated that casting material estimation as a conditional latent diffusion process, leveraging knowledge from large pre-trained diffusion models like Stable Diffusion [33], is effective. However, for our task that requires simultaneous generation of multiple material maps, three key issues remain: 1) High model overhead: Fine-tuning Stable Diffusion with its original architecture can only estimate a single material type. Even when combining metallic and roughness into an RM map, treating it as a single material still requires two diffusion models, one for albedo and another for RM, to meet the rendering model’s requirements. This results in doubled training time and increased inference space overhead. 2) Slow inference speed: With the widely used DDIM scheduler, diffusion models

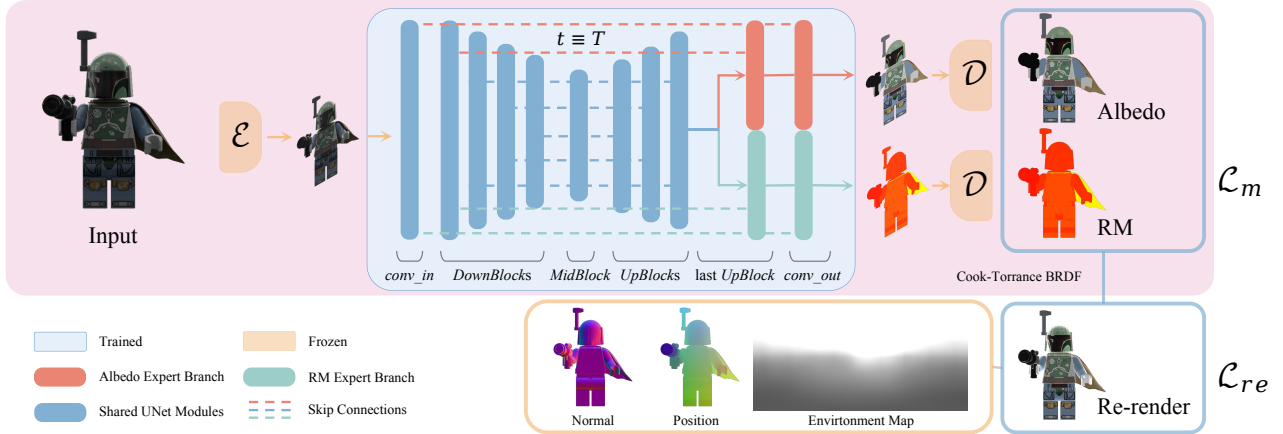


Figure 2. Overview of the SuperMat framework. The UNet architecture incorporates structural expert branches for albedo and RM estimation, enabling parallel material property prediction while sharing a common backbone. During training, we leverage a fixed DDIM scheduler and optimize the network end-to-end using both perceptual loss and re-render loss. The marked region shows the inference pipeline, where our model achieves single-step inference for concurrent material map generation. Input geometric information (normal, position) and environment maps are used to compute the re-render loss.

require 30 to 50 denoising steps to produce satisfactory results, which can be inefficient and time-consuming. 3) Incomplete decomposition effect: Due to the high computational cost of backpropagation in multi-step inference, prior diffusion-based methods trained on predicted noise from single-step denoising rather than directly supervising the fully denoised material output. This limitation restricts the model’s ability to specialize in the decomposition task and impedes the application of more task-specific techniques.

Structural Expert Branches. Our solution to the first problem is to introduce a structural expert branch architecture [24]. Previous methods are limited to using a single diffusion model to estimate one material type. Although training separate models for different material maps is an intuitive approach, it introduces issues such as implementation complexity, high overhead, and inconsistencies between materials. Considering that, despite their different representations, materials fundamentally reflect an understanding of object features, we incorporate structural expert branches into the UNet model, allowing a single diffusion model to predict multiple material maps. Specifically, we design two expert branches, one for predicting albedo, and the other for predicting RM. For each expert branch, we replicate the UNet’s last *UpBlock*, and *conv_out*, while the rest of the UNet architecture remains shared between the branches. The modified model first extracts and transforms encoded image features through the shared modules. These features are then separated into 2 copies by duplicating before the last *UpBlock*, with each branch ultimately predicting results for its respective domain. The expert branches specialize in material-specific features, while the shared modules focus on commonalities. In this way, we

only add a small number of parameters, achieving the same performance as previous methods that would otherwise require twice the scale.

Single-Step Inference and End-to-End Training. To address the second problem, we analyze the DDIM scheduler of diffusion models. Previous works have highlighted a flaw in the implementation of the DDIM scheduler [12, 22], which limits the potential of single-step inference in Stable Diffusion: In the default leading timestep setting of DDIM, for single-step prediction, the model is provided with a timestep ($t=1$) suggesting the input is essentially denoised, yet in reality, the input is pure noise. The discrepancy between the timestep and the actual noise level causes the single-step result to be flawed. To align the timestep with the noise level received by the model, we adjust the scheduler to use the trailing setting ($t=T$ for single-step), correcting this issue and enabling single-step inference, significantly reducing the time overhead.

More importantly, after this correction, we can fine-tune the one-step model end-to-end, effectively resolving the third issue. For a diffusion model with the uncorrected timestep setting, fine-tuning the diffusion model end-to-end is impractical, because generating a clean material map typically requires multiple denoising steps, leading to prohibitive computational complexity due to the gradient calculations. As an alternative, previous methods [5, 23, 41] rely on using the noise latent obtained from a single denoising step of the UNet for loss calculation. However, this approach shifts the model’s training objective from material decomposition to general image denoising, which hinders specialization for this task. In contrast, our corrected inference pipeline can generate fully denoised material maps in

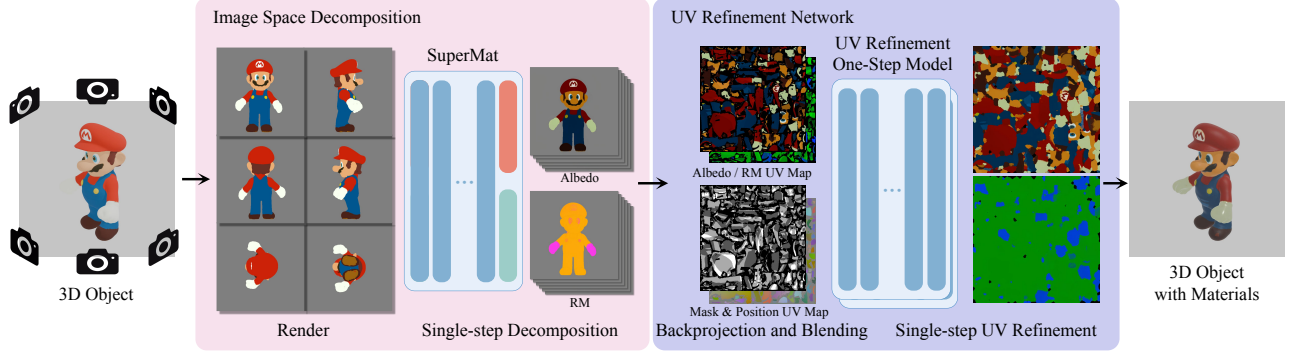


Figure 3. Material Decomposition for 3D objects. Applying SuperMat’s powerful decomposition to 3D objects, we can obtain an object with high-quality materials in just three inference steps.

a single denoising step, making end-to-end fine-tuning both feasible and efficient for material decomposition. Specifically, with the clean material estimations, we compute perceptual losses [17] between the predicted albedo map k_d , the RM map k_{rm} , and the ground truth maps \hat{k}_d, \hat{k}_{rm} :

$$\mathcal{L}_p(\hat{y}, y) = \sum_j \frac{1}{C_j H_j W_j} \|\phi_j(\hat{y}) - \phi_j(y)\|_1, \quad (2)$$

$$\mathcal{L}_m = \mathcal{L}_p(\hat{k}_d, k_d) + \mathcal{L}_p(\hat{k}_{rm}, k_{rm}),$$

where ϕ is a 16-layer VGG network, and ϕ_j represents the output of the j -th layer, with a shape of $C_j \times H_j \times W_j$. In this paper, we use the 4th, 8th, 12th, and 16th layers to compute the feature reconstruction loss.

Note that, following the approach of previous work [12], we use “Zeros” as the noise type during fine-tuning, meaning no random noise is added.

Re-render Loss in DM Fine-tuning. Data-driven decomposition diffusion models typically focus on the distribution of individual material maps, yet they often overlook the interactions between different types of material maps. In other words, previous methods compute the loss between the predicted values and the ground truth without utilizing material information for further operations or calculations, which could provide stronger guidance for the model. As a result, although the predicted materials may appear close to the ground truth, the rendered output may not align with expectations. While this can be frustrating, it is understandable, as their training methods only produce meaningless predicted noise at each iteration. In contrast, our design, which incorporates structural expert branches and single-step prediction, allows us to obtain all denoised material maps during the training iterations. Using this information, we introduce the re-render loss, which involves rendering the model in a new lighting environment and comparing the result to the ground truth. Specifically, at each training iteration, we obtain $k_d, k_{rm} = (k_r, k_m)$, along with the true nor-

mal map \hat{k}_n , position map \hat{k}_p , camera viewpoint \hat{c} , and an environment light map. Then we use these information and the rendering model \mathcal{R} described in Sec. 3.1 to compute the predicted material’s performance under new illumination. Similarly, with the groundtruth albedo \hat{k}_d and RM \hat{k}_{rm} , we compute the ground truth of relighting. The perceptual loss between these two renderings defines our re-render loss:

$$\mathcal{L}_{re} = \mathcal{L}_p(\mathcal{R}_{\hat{k}_n, \hat{k}_p, \hat{c}}(\hat{k}_d, \hat{k}_m, \hat{k}_r), \mathcal{R}_{\hat{k}_n, \hat{k}_p, \hat{c}}(k_d, k_m, k_r)). \quad (3)$$

3.3. UV Refinement Network

We aim to apply SuperMat to decompose material for 3D objects with only RGB textures. Several previous works [4, 29, 35, 45] use techniques like SDS to bridge the gap between dimensions, but such methods are not applicable to our deterministic model, and suffer from slow computational speed and mode seeking issues. Therefore, we explore using backprojection to transfer 2D decomposition results from image space to UV space, enabling their application to 3D models. Notably, SuperMat is a single-view model, meaning that one inference can only decompose the visible region from a single viewpoint. To address this problem, we propose estimating materials from multiple viewpoints and integrating them. With multi-view decomposition results from SuperMat, the UV refinement network aims at inpainting missing areas, eliminating discrepancies between different views, and improving the overall quality of the generated materials.

Backprojection and UV Blending. For each viewpoint, we backproject SuperMat’s decomposition results from image space onto the model’s UV texture map, obtaining the partial albedo UV map C_d^i , RM UV map C_{rm}^i , and mask UV map M^i for viewpoint i . We then blend the backprojection results from all viewpoints in an averaged manner.

	Albedo			Metallic			Roughness			Relighting			Time(s)↓
	PSNR↑	SSIM↑	LPIPS↓	PSNR↑	SSIM↑	LPIPS↓	PSNR↑	SSIM↑	LPIPS↓	PSNR↑	SSIM↑	LPIPS↓	
Derender3D [36]	22.2606	0.8724	0.1622	-	-	-	-	-	-	-	-	-	0.16
IIR [47]	20.9665	0.8679	0.1629	16.8817	0.8118	0.2364	19.9573	0.8749	0.1578	21.5253	0.8901	0.1279	0.04
IID [20]	22.8717	0.8881	0.1304	17.3730	0.8086	0.2410	20.7641	0.8818	0.1380	23.3206	0.9077	0.1023	1.45
RGB→X [41]	20.1181	0.8837	0.1407	16.0954	0.8077	0.2638	20.9801	0.8880	0.1376	20.8278	0.8973	0.1119	3.32
IntrinsicAnything [5]	20.7927	0.8721	0.1582	-	-	-	-	-	-	-	-	-	6.93
StableMaterial [23]	23.8992	0.9050	0.1032	15.9797	0.8128	0.2548	18.2711	0.8535	0.1712	22.1842	0.8974	0.1045	0.53
Ours w/o e2e	24.6155	0.8966	0.1102	19.8342	0.8576	0.2321	20.8168	0.8769	0.1391	24.3308	0.9125	0.0899	3.09
Ours w/o re-render	27.2149	0.9219	0.0862	22.9245	0.8474	0.1968	23.3083	0.9043	0.1122	26.7900	0.9341	0.0687	0.07
Ours	27.5034	0.9240	0.0845	23.4598	0.8598	0.1937	23.5158	0.9040	0.1114	27.1192	0.9366	0.0640	0.07

Table 1. Comparison of our method with others on the image space decomposition task. We highlight the **best**, **second-best**, and **third-best** results for each metric. "Ours w/o e2e" denotes our method without the scheduler fix and perceptual loss for end-to-end training. "Ours w/o re-render" denotes our method without the re-render loss. The first three methods are non-diffusion-based, while the middle three methods are diffusion-based.

For albedo, this can be formulated as:

$$M = \sum_i M^i, \quad (4)$$

$$C_d = \frac{\sum_i C_d^i}{(M + \epsilon)}.$$

The RM follows the same computation method. The blended partial maps C_d , C_{rm} , and the partial mask M are then input into the subsequent UV refinement one-step model.

UV Refinement One-Step Model. Due to the limited number of viewpoints, the blended partial maps often have missing areas. Additionally, slight variances may exist between SuperMat’s results from different views. To address these issues, we leverage diffusion models for UV refinement: we fine-tune Stable Diffusion into a UV refinement model, which takes a flawed partial material UV map, a mask UV map, and a position UV map as inputs, and outputs completed, variance-corrected, and refined material UV maps. Specifically, the material maps are encoded by a VAE and concatenated with downsampled mask and position maps, and then processed by UNet with an expanded 8-channel *conv_in*. We also modify the model’s scheduler to support single-step inference and enable end-to-end training, resulting a deterministic one-step model.

Material Decomposition Pipeline for 3D Objects. As shown in Fig. 3, with the fine-tuned UV refinement network, we propose a complete pipeline for the material decomposition of 3D objects. Given an object with only RGB texture, we first render it from six orthogonal viewpoints. The rendered results are then batch-processed by SuperMat for material decomposition. These materials, including albedo and RM, are backprojected into UV space and blended. The blended partial maps are then refined by the UV refinement one-step model and the final material UV maps are generated. This process requires only three inference steps—one

for SuperMat, one for refining albedo, and one for refining RM—allowing our pipeline to complete the material decomposition of a 3D object in just 3 seconds.

4. Experiments

Quantitative Comparison of Image Space Decomposition. We randomly select 64 unseen items each from the Objaverse [8] and BlenderVault [23] datasets. Our method is tested against 6 baseline approaches on these 128 objects. For each object, the model processes 18 inputs corresponding to 3 lighting conditions and 6 viewpoints, predicting 3 (or 1) types of materials and generating 54 (or 18) texture maps in total. All outputs are used to compute metrics, with the final averaged results shown in Tab.1. We use PSNR, SSIM, and LPIPS metrics to evaluate albedo, metallic, and roughness. Additionally, for methods that provide all material types, we compute metrics on the rendering under relighting conditions using the ground truth normals and positions and the predicted values. The results demonstrate that our approach significantly outperforms the state-of-the-art in image space decomposition.

Beyond image quality, we compare inference speeds by calculating the total time required for each method to process the test set, normalized by the dataset size and number of predicted material types. All tests are conducted with a batch size of 1. For consistency in speed comparison, StableMaterial and IID, which typically average over 10 predictions per input, are modified to perform a single prediction. The "Time(s)" column in Tab.1 reflects the time required by each method to generate a single material prediction on an NVIDIA A100 GPU with a batch size of 1. Traditional, non-diffusion-based methods like Derender3D, IIR, and IID generally show faster speeds. While StableMaterial attempts to predict multiple materials simultaneously by adding extra channels to *conv_in* and *conv_out*, its lack of structural design adjustments limits prediction qual-

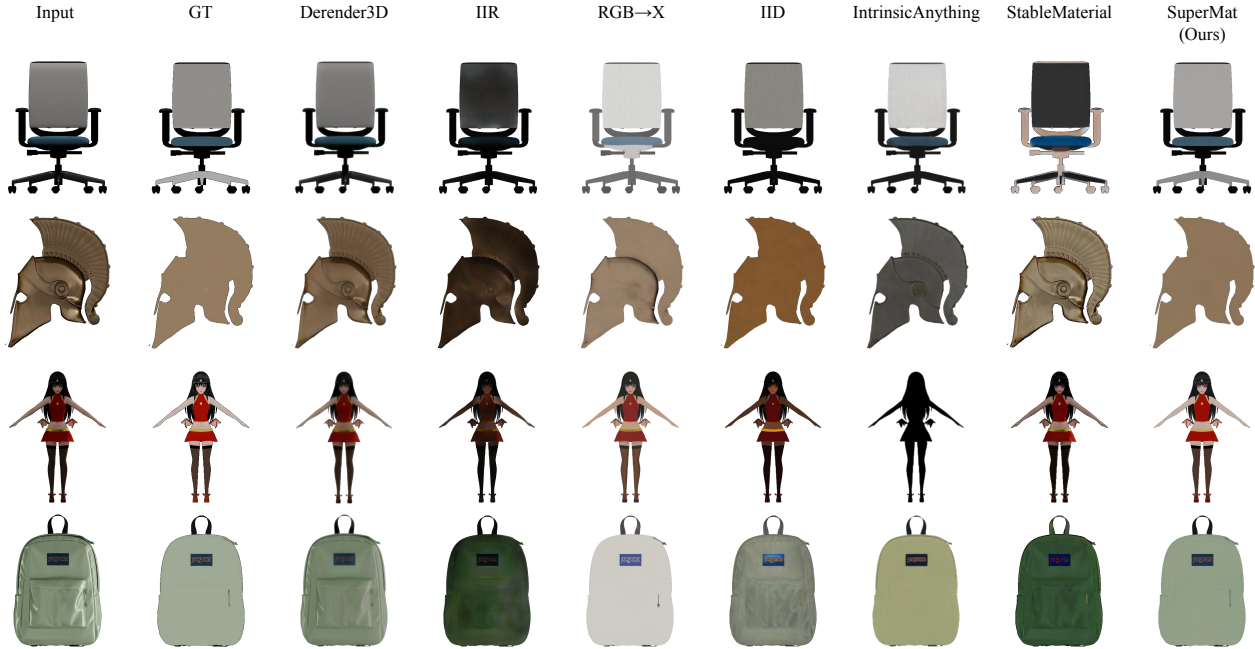


Figure 4. Comparison of our method with others on albedo estimation results.

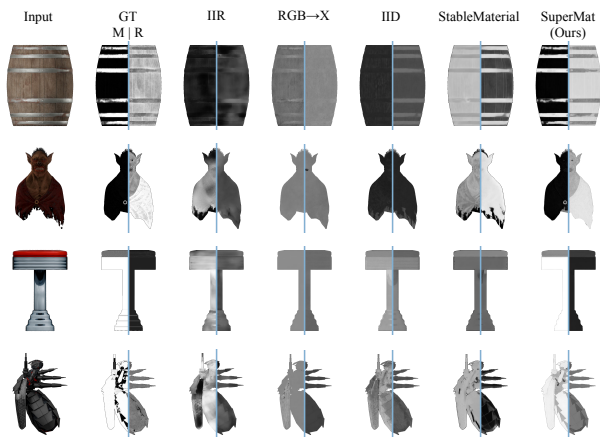


Figure 5. Comparison of our method with others on metallic and roughness estimation results. We combined both materials into a single image, with the left half representing metallic and the right half showing roughness. It can be observed that these two materials exhibit more variation and are more challenging to estimate compared to albedo.

ity and requires multi-step denoising, resulting in slower performance than traditional methods. In contrast, our approach achieves high-quality material decomposition with speeds comparable to traditional methods.

Qualitative Comparison of Image Space Decomposition. Fig.4 compares albedo prediction results across various cases, including artist-designed objects and real-world

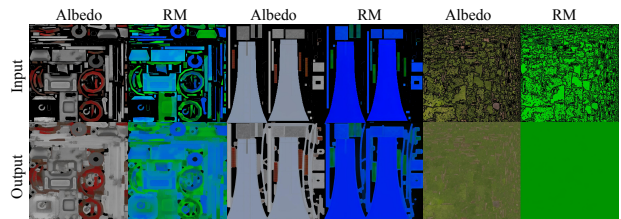


Figure 6. Results of UV refinement one-step model.

scans, showcasing the performance of our method against other approaches. SuperMat demonstrates superior ability in removing highlights and shadows, accurately capturing the intrinsic color, even on challenging metallic surfaces. In Fig.5, we present metallic and roughness predictions from our method alongside other baselines. SuperMat outperforms the others with well-defined boundaries between metallic and non-metallic regions and achieves consistency within material types while preserving high-frequency details. Moreover, our results closely align with physical realism, addressing a significant challenge that previous methods struggled to overcome. Results with a wider variety of inputs will be presented in the supplementary materials.

Results of UV Refinement and Material Estimation for 3D Objects. Fig.6 illustrates the effectiveness of the UV refinement one-step model in inpainting missing areas and harmonizing viewpoint variances in SuperMat’s outputs. Fig.8 displays the results from our material es-

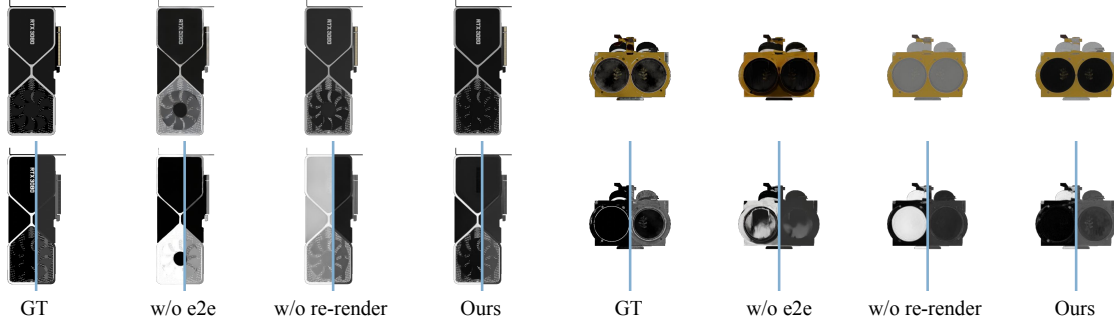


Figure 7. Qualitative ablation results for SuperMat. The first row shows albedo, while the second row shows metallic and roughness.

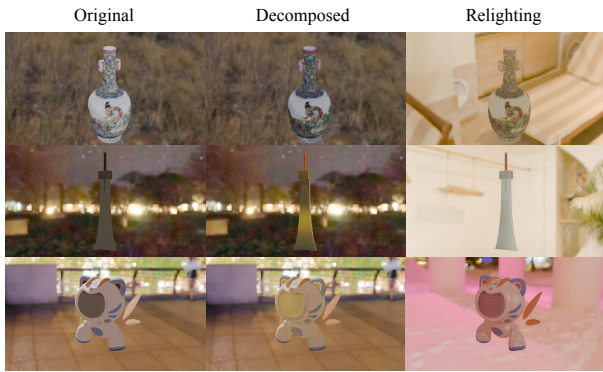


Figure 8. Results of decomposition for 3D objects. We show the comparison between the original and decomposed models under the same environment map, along with the relighting outcomes of new models.

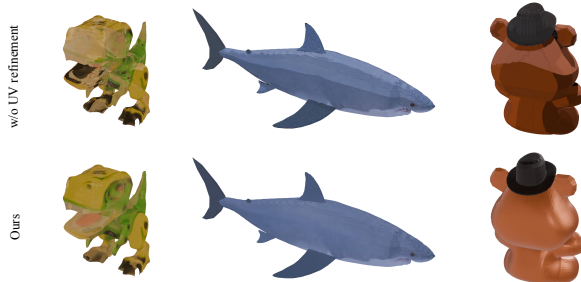


Figure 9. Qualitative ablation results on UV refinement network.

timation pipeline for 3D models. The first column shows the rendering of the input models with only RGB texture, where all surfaces exhibit uniform reflectance behavior. After applying our method, the decomposed materials enable physically-based rendering with surface-specific reflectance properties, as demonstrated in the second and third columns under different lighting conditions.

Ablation Studies. In Tab.1, we present ablation studies on two core components of SuperMat: end-to-end (e2e) training and re-render loss. E2E with perceptual loss signifi-

cantly enhances model performance and efficiency. In fact, within the e2e framework, we experiment with three types of loss functions, with perceptual loss achieving the best results. This suggests that direct supervision of the fully denoised predicted material maps, rather than latent noise, plays a critical role in enhancing the model’s capability for this specific task. Detailed findings are available in the supplementary materials. The addition of re-render loss, facilitated by the e2e framework, further improves prediction quality, particularly under relighting conditions. Qualitative results of these ablations are shown in Fig. 7. The ‘w/o e2e’ setting, where the model is trained without perceptual and re-render losses, limits its capacity to remove lighting effects effectively. In contrast, training ‘w/o re-render’ loss leads to minor inaccuracies in fine material details. Note that in the ‘w/o e2e’ setting, there are slight differences in the implementation of the UNet. Detailed explanations will be provided in the supplementary materials.

For the decomposition pipeline for 3D objects, we conduct additional ablations on the UV refinement network. Due to limitations from only six orthogonal views, achieving complete texture coverage, accurate merging of overlapping regions, and consistent material transitions are challenging. As shown in Fig.9, omitting the UV refinement leads to incomplete textures, visible color-separation lines, and unnatural transitions between materials, underscoring the importance of this component.

5. Conclusions

In this paper, we present SuperMat, an innovative image space material decomposition one-step model fine-tuned from Stable Diffusion with task-specific losses in an end-to-end framework. SuperMat enables simultaneous multi-material prediction and supports single-step inference, achieving state-of-the-art quality and outperforming previous diffusion-based methods in efficiency. Through the proposed UV refinement network, we extend SuperMat to decomposition tasks for 3D objects, where it demonstrates exceptional performance and applicability.

References

- [1] Raphael Bensch, Yanir Kleiman, Idan Azuri, Omri Harosh, Andrea Vedaldi, Natalia Neverova, and Oran Gafni. Meta 3d texturegen: Fast and consistent texture generation for 3d objects. *arXiv preprint arXiv:2407.02430*, 2024. 3
- [2] Mark Boss, Varun Jampani, Raphael Braun, Ce Liu, Jonathan Barron, and Hendrik Lensch. Neural-pil: Neural pre-integrated lighting for reflectance decomposition. *Advances in Neural Information Processing Systems*, 34: 10691–10704, 2021. 2
- [3] Dave Zhenyu Chen, Yawar Siddiqui, Hsin-Ying Lee, Sergey Tulyakov, and Matthias Nießner. Text2tex: Text-driven texture synthesis via diffusion models. In *Proceedings of the IEEE/CVF International Conference on Computer Vision*, pages 18558–18568, 2023. 3
- [4] Rui Chen, Yongwei Chen, Ningxin Jiao, and Kui Jia. Fantasia3d: Disentangling geometry and appearance for high-quality text-to-3d content creation. In *Proceedings of the IEEE/CVF International Conference on Computer Vision (ICCV)*, 2023. 3, 5
- [5] Xi Chen, Sida Peng, Dongchen Yang, Yuan Liu, Bowen Pan, Chengfei Lv, and Xiaowei Zhou. Intrinsicanything: Learning diffusion priors for inverse rendering under unknown illumination. *arXiv preprint arXiv:2404.11593*, 2024. 1, 2, 3, 4, 6
- [6] Ziang Cheng, Junxuan Li, and Hongdong Li. Wildlight: In-the-wild inverse rendering with a flashlight. In *Proceedings of the IEEE/CVF Conference on Computer Vision and Pattern Recognition*, pages 4305–4314, 2023. 2
- [7] Robert L Cook and Kenneth E. Torrance. A reflectance model for computer graphics. *ACM Transactions on Graphics (ToG)*, 1(1):7–24, 1982. 3
- [8] Matt Deitke, Dustin Schwenk, Jordi Salvador, Luca Weihs, Oscar Michel, Eli VanderBilt, Ludwig Schmidt, Kiana Ehsani, Aniruddha Kembhavi, and Ali Farhadi. Objaverse: A universe of annotated 3d objects. In *Proceedings of the IEEE/CVF Conference on Computer Vision and Pattern Recognition*, pages 13142–13153, 2023. 6, 1
- [9] Yiqun Duan, Xianda Guo, and Zheng Zhu. Diffusiondepth: Diffusion denoising approach for monocular depth estimation. *arXiv preprint arXiv:2303.05021*, 3, 2023. 3
- [10] Xiao Fu, Wei Yin, Mu Hu, Kaixuan Wang, Yuexin Ma, Ping Tan, Shaojie Shen, Dahua Lin, and Xiaoxiao Long. Geowizard: Unleashing the diffusion priors for 3d geometry estimation from a single image. In *European Conference on Computer Vision*, pages 241–258. Springer, 2025. 3
- [11] Jian Gao, Chun Gu, Youtian Lin, Hao Zhu, Xun Cao, Li Zhang, and Yao Yao. Relightable 3d gaussian: Real-time point cloud relighting with brdf decomposition and ray tracing. *arXiv preprint arXiv:2311.16043*, 2023. 2
- [12] Gonzalo Martin Garcia, Karim Abou Zeid, Christian Schmidt, Daan de Geus, Alexander Hermans, and Bastian Leibe. Fine-tuning image-conditional diffusion models is easier than you think. *arXiv preprint arXiv:2409.11355*, 2024. 2, 3, 4, 5
- [13] Ming Gui, Johannes S Fischer, Ulrich Prestel, Pingchuan Ma, Dmytro Kotovenko, Olga Grebenkova, Stefan Andreas Baumann, Vincent Tao Hu, and Björn Ommer. Depthfm: Fast monocular depth estimation with flow matching. *arXiv preprint arXiv:2403.13788*, 2024. 3
- [14] Yuan-Chen Guo, Di Kang, Linchao Bao, Yu He, and Song-Hai Zhang. Nerfren: Neural radiance fields with reflections. In *Proceedings of the IEEE/CVF Conference on Computer Vision and Pattern Recognition*, pages 18409–18418, 2022. 2
- [15] Jon Hasselgren, Nikolai Hofmann, and Jacob Munkberg. Shape, light, and material decomposition from images using monte carlo rendering and denoising. *Advances in Neural Information Processing Systems*, 35:22856–22869, 2022. 2
- [16] Haian Jin, Isabella Liu, Peijia Xu, Xiaoshuai Zhang, Songfang Han, Sai Bi, Xiaowei Zhou, Zexiang Xu, and Hao Su. Tensorir: Tensorial inverse rendering. In *Proceedings of the IEEE/CVF Conference on Computer Vision and Pattern Recognition*, pages 165–174, 2023. 2
- [17] Justin Johnson, Alexandre Alahi, and Li Fei-Fei. Perceptual losses for real-time style transfer and super-resolution. In *Computer Vision—ECCV 2016: 14th European Conference, Amsterdam, The Netherlands, October 11–14, 2016, Proceedings, Part II 14*, pages 694–711. Springer, 2016. 5
- [18] Bingxin Ke, Anton Obukhov, Shengyu Huang, Nando Metzger, Rodrigo Caye Daudt, and Konrad Schindler. Repurposing diffusion-based image generators for monocular depth estimation. In *Proceedings of the IEEE/CVF Conference on Computer Vision and Pattern Recognition*, pages 9492–9502, 2024. 3
- [19] Alexander Kirillov, Eric Mintun, Nikhila Ravi, Hanzi Mao, Chloe Rolland, Laura Gustafson, Tete Xiao, Spencer Whitehead, Alexander C Berg, Wan-Yen Lo, et al. Segment anything. In *Proceedings of the IEEE/CVF International Conference on Computer Vision*, pages 4015–4026, 2023. 6
- [20] Peter Kocsis, Vincent Sitzmann, and Matthias Nießner. Intrinsic image diffusion for indoor single-view material estimation. In *Proceedings of the IEEE/CVF Conference on Computer Vision and Pattern Recognition*, pages 5198–5208, 2024. 2, 6, 1
- [21] Zhihao Liang, Qi Zhang, Ying Feng, Ying Shan, and Kui Jia. Gs-ir: 3d gaussian splatting for inverse rendering. In *Proceedings of the IEEE/CVF Conference on Computer Vision and Pattern Recognition*, pages 21644–21653, 2024. 2
- [22] Shanchuan Lin, Bingchen Liu, Jiashi Li, and Xiao Yang. Common diffusion noise schedules and sample steps are flawed. In *Proceedings of the IEEE/CVF winter conference on applications of computer vision*, pages 5404–5411, 2024. 3, 4
- [23] Yehonathan Litman, Or Patashnik, Kangle Deng, Aviral Agrawal, Rushikesh Zawar, Fernando De la Torre, and Shubham Tulsiani. Materialfusion: Enhancing inverse rendering with material diffusion priors. *arXiv preprint arXiv:2409.15273*, 2024. 1, 2, 3, 4, 6
- [24] Xian Liu, Jian Ren, Aliaksandr Siarohin, Ivan Skorokhodov, Yanyu Li, Dahua Lin, Xihui Liu, Ziwei Liu, and Sergey Tulyakov. Hyperhuman: Hyper-realistic human generation with latent structural diffusion. *arXiv preprint arXiv:2310.08579*, 2023. 2, 3, 4

- [25] Yunfei Liu, Yu Li, Shaodi You, and Feng Lu. Unsupervised learning for intrinsic image decomposition from a single image. In *Proceedings of the IEEE/CVF conference on computer vision and pattern recognition*, pages 3248–3257, 2020. 2
- [26] Yuxin Liu, Minshan Xie, Hanyuan Liu, and Tien-Tsin Wong. Text-guided texturing by synchronized multi-view diffusion. *arXiv preprint arXiv:2311.12891*, 2023. 3
- [27] Jacob Munkberg, Jon Hasselgren, Tianchang Shen, Jun Gao, Wenzheng Chen, Alex Evans, Thomas Müller, and Sanja Fidler. Extracting triangular 3d models, materials, and lighting from images. In *Proceedings of the IEEE/CVF Conference on Computer Vision and Pattern Recognition*, pages 8280–8290, 2022. 2, 3
- [28] Maxime Oquab, Timothée Darcet, Théo Moutakanni, Huy Vo, Marc Szafraniec, Vasil Khalidov, Pierre Fernandez, Daniel Haziza, Francisco Massa, Alaaeldin El-Nouby, et al. Dinov2: Learning robust visual features without supervision. *arXiv preprint arXiv:2304.07193*, 2023. 1
- [29] Ben Poole, Ajay Jain, Jonathan T Barron, and Ben Mildenhall. Dreamfusion: Text-to-3d using 2d diffusion. *arXiv preprint arXiv:2209.14988*, 2022. 3, 5
- [30] Lingteng Qiu, Guanying Chen, Xiaodong Gu, Qi Zuo, Mutian Xu, Yushuang Wu, Weihao Yuan, Zilong Dong, Liefeng Bo, and Xiaoquang Han. Richdreamer: A generalizable normal-depth diffusion model for detail richness in text-to-3d. In *Proceedings of the IEEE/CVF Conference on Computer Vision and Pattern Recognition*, pages 9914–9925, 2024. 3
- [31] René Ranftl, Katrin Lasinger, David Hafner, Konrad Schindler, and Vladlen Koltun. Towards robust monocular depth estimation: Mixing datasets for zero-shot cross-dataset transfer. *IEEE transactions on pattern analysis and machine intelligence*, 44(3):1623–1637, 2020. 1
- [32] Elad Richardson, Gal Metzer, Yuval Alaluf, Raja Giryes, and Daniel Cohen-Or. Texture: Text-guided texturing of 3d shapes. In *ACM SIGGRAPH 2023 conference proceedings*, pages 1–11, 2023. 3
- [33] Robin Rombach, Andreas Blattmann, Dominik Lorenz, Patrick Esser, and Björn Ommer. High-resolution image synthesis with latent diffusion models. In *Proceedings of the IEEE/CVF conference on computer vision and pattern recognition*, pages 10684–10695, 2022. 3
- [34] Saurabh Saxena, Abhishek Kar, Mohammad Norouzi, and David J Fleet. Monocular depth estimation using diffusion models. *arXiv preprint arXiv:2302.14816*, 2023. 3
- [35] Zhengyi Wang, Cheng Lu, Yikai Wang, Fan Bao, Chongxuan Li, Hang Su, and Jun Zhu. Prolificdreamer: High-fidelity and diverse text-to-3d generation with variational score distillation. *Advances in Neural Information Processing Systems*, 36, 2024. 3, 5
- [36] Felix Wimbauer, Shangzhe Wu, and Christian Rupprecht. De-rendering 3d objects in the wild. In *Proceedings of the IEEE/CVF Conference on Computer Vision and Pattern Recognition*, pages 18490–18499, 2022. 2, 6, 1
- [37] Guangkai Xu, Yongtao Ge, Mingyu Liu, Chengxiang Fan, Kangyang Xie, Zhiyue Zhao, Hao Chen, and Chunhua Shen. Diffusion models trained with large data are transferable visual models. *arXiv preprint arXiv:2403.06090*, 2024. 2
- [38] Chongjie Ye, Lingteng Qiu, Xiaodong Gu, Qi Zuo, Yushuang Wu, Zilong Dong, Liefeng Bo, Yuliang Xiu, and Xiaoquang Han. Stablenormal: Reducing diffusion variance for stable and sharp normal. *arXiv preprint arXiv:2406.16864*, 2024. 3
- [39] Renjiao Yi, Chenyang Zhu, and Kai Xu. Weakly-supervised single-view image relighting. In *Proceedings of the IEEE/CVF Conference on Computer Vision and Pattern Recognition*, pages 8402–8411, 2023. 2
- [40] Xianfang Zeng, Xin Chen, Zhongqi Qi, Wen Liu, Zibo Zhao, Zhibin Wang, Bin Fu, Yong Liu, and Gang Yu. Paint3d: Paint anything 3d with lighting-less texture diffusion models. In *Proceedings of the IEEE/CVF Conference on Computer Vision and Pattern Recognition*, pages 4252–4262, 2024. 3
- [41] Zheng Zeng, Valentin Deschaintre, Iliyan Georgiev, Yannick Hold-Geoffroy, Yiwei Hu, Fujun Luan, Ling-Qi Yan, and Miloš Hašan. Rgb \leftrightarrow x: Image decomposition and synthesis using material-and lighting-aware diffusion models. In *ACM SIGGRAPH 2024 Conference Papers*, pages 1–11, 2024. 1, 2, 3, 4, 6
- [42] Kai Zhang, Fujun Luan, Zhengqi Li, and Noah Snavely. Iron: Inverse rendering by optimizing neural sdfs and materials from photometric images. In *Proceedings of the IEEE/CVF Conference on Computer Vision and Pattern Recognition*, pages 5565–5574, 2022. 2
- [43] Xiuming Zhang, Pratul P Srinivasan, Boyang Deng, Paul Debevec, William T Freeman, and Jonathan T Barron. Nerfactor: Neural factorization of shape and reflectance under an unknown illumination. *ACM Transactions on Graphics (TOG)*, 40(6):1–18, 2021. 2
- [44] Yuanqing Zhang, Jiaming Sun, Xingyi He, Huan Fu, Rongfei Jia, and Xiaowei Zhou. Modeling indirect illumination for inverse rendering. In *Proceedings of the IEEE/CVF Conference on Computer Vision and Pattern Recognition*, pages 18643–18652, 2022. 2
- [45] Yuqing Zhang, Yuan Liu, Zhiyu Xie, Lei Yang, Zhongyuan Liu, Mengzhou Yang, Runze Zhang, Qilong Kou, Cheng Lin, Wenping Wang, et al. Dreammat: High-quality pbr material generation with geometry-and light-aware diffusion models. *ACM Transactions on Graphics (TOG)*, 43(4):1–18, 2024. 3, 5
- [46] Wenliang Zhao, Yongming Rao, Zuyan Liu, Benlin Liu, Jie Zhou, and Jiwen Lu. Unleashing text-to-image diffusion models for visual perception. In *Proceedings of the IEEE/CVF International Conference on Computer Vision*, pages 5729–5739, 2023. 3
- [47] Jingsen Zhu, Fujun Luan, Yuchi Huo, Zihao Lin, Zhihua Zhong, Dianbing Xi, Rui Wang, Hujun Bao, Jiayang Zheng, and Rui Tang. Learning-based inverse rendering of complex indoor scenes with differentiable monte carlo raytracing. In *SIGGRAPH Asia 2022 Conference Papers*, pages 1–8, 2022. 2, 6, 1

SuperMat: Physically Consistent PBR Material Estimation at Interactive Rates

Supplementary Material

6. Additional Details

Implementation Details. We report some implementation details as follows: 1) In the UV refinement one-step model, the input channels are expanded to 8, with the weights of the additional 4 channels initialized to 0. 2) In the ablation experiment, the structure of SuperMat under the “w/o e2e” setting is slightly different. Without single-step inference, we can only train the diffusion model in a denoising task manner, meaning that during the single-step denoising process, the latents that the UNet receives are not encoded from a clean rendered image, but rather a noisy albedo and noisy RM. Therefore, on top of SuperMat, we additionally replicate the *conv.in* and the first *DownBlock* as independent parts of structural expert branches to map the inputs from two different domains to similar distributions. These are then fused in an averaged manner before being fed into the shared modules. 3) In the re-render loss implementation, each time we perform relighting, we randomly select a lighting condition from a set of 716 environment maps, covering nearly all possible lighting scenarios.

Training Details. Both models are fine-tuned from Stable Diffusion 2.1. We train SuperMat using the AdamW optimizer with a learning rate of $1e - 5$ on 8 NVIDIA A800 (80GB) GPUs, with a batch size of 16, for a total of 115 epochs. The UV refinement one-step model is trained with the AdamW optimizer at a learning rate of $2e - 5$, also on 8 NVIDIA A800 (80GB) GPUs, with a batch size of 16, for 40 epochs. The images are resized to resolutions of 512×512 and 1024×1024 , used for SuperMat and the UV refinement one-step model, respectively.

Training Datasets. In this paper, we collect 3D objects from Objaverse [8]. For each object, we render material maps, normal maps, and position maps from six orthogonal viewpoints and generate PBR results under three different environment lighting conditions from the same viewpoints. We then filter high-quality data using methods such as DINO score considerations [28], resulting in a dataset of 100k objects for the image space decomposition task. Following the approach outlined in Sec. 3.3, we further refine this data for the UV refinement network by selecting cases where the missing area in blended partial UV maps is under 50%. This process results in a final dataset of 40k objects for training the refinement one-step model.

Image Space Decomposition Baselines. We compare SuperMat with 6 other image space decomposition networks. Inverse Indoor Rendering (IIR) [47], Intrinsic Image Diffusion (IID) [20], and RGB→X [41] are scene-level material estimation methods. Derender3D [36] and Intrinsic

Anything [5] are adaptable to diverse data but do not generate all material types. StableMaterial [23] provides image space material denoising diffusion priors to MaterialFusion, and, like SuperMat, focuses on decomposing object materials.

7. Additional Visualizations

In Figures 10, 11, 12, 13, we present additional results of SuperMat on the Objaverse and BlenderVault test datasets, covering both artist-designed and real-world scanned objects. Fig. 14 highlights more decomposition results of real-world objects extracted from captured images. Finally, Fig. 15 illustrates more decomposition results on 3D objects.

8. Additional Experiments

We show the detailed quantitative comparison in Tables 3, 4, 5 and 6. Additionally, without re-render loss, we experiment with three types of loss functions in the end-to-end framework: L1 loss, shift and scale invariant (SSI) loss [31], and perceptual loss. The performance of models trained with these loss designs is evaluated on the same test dataset, and the results are shown in Tab. 2. Among these losses, the perceptual loss, which is ultimately adopted by SuperMat, demonstrates the best performance.



Figure 10. Additional albedo comparison from the Objaverse test dataset.

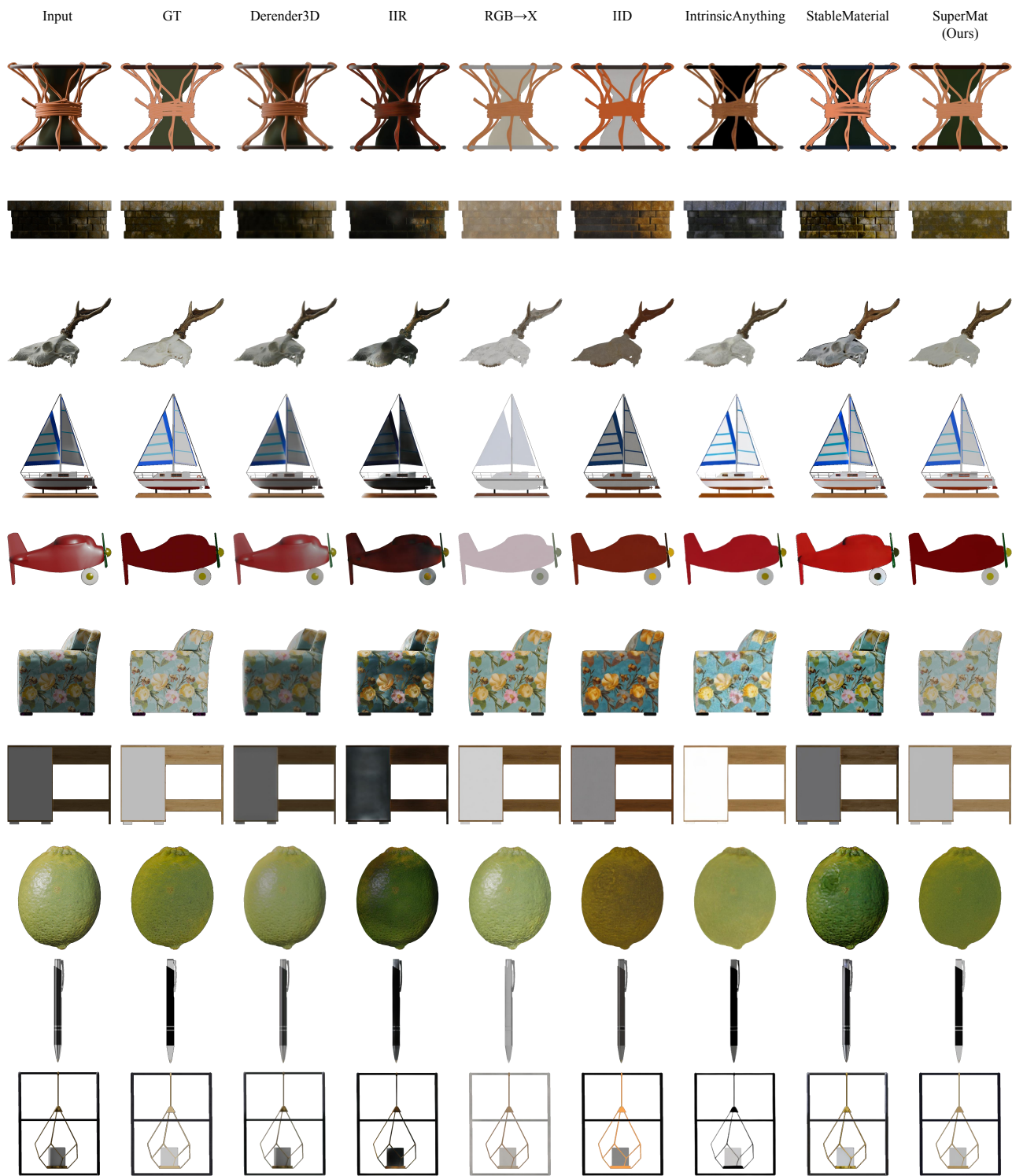


Figure 11. Additional albedo comparison from the BlenderVault test dataset.



Figure 12. Additional metallic and roughness comparison from the Objaverse test dataset. The metallic maps are shown on the left side (M), while the roughness maps are shown on the right side (R).

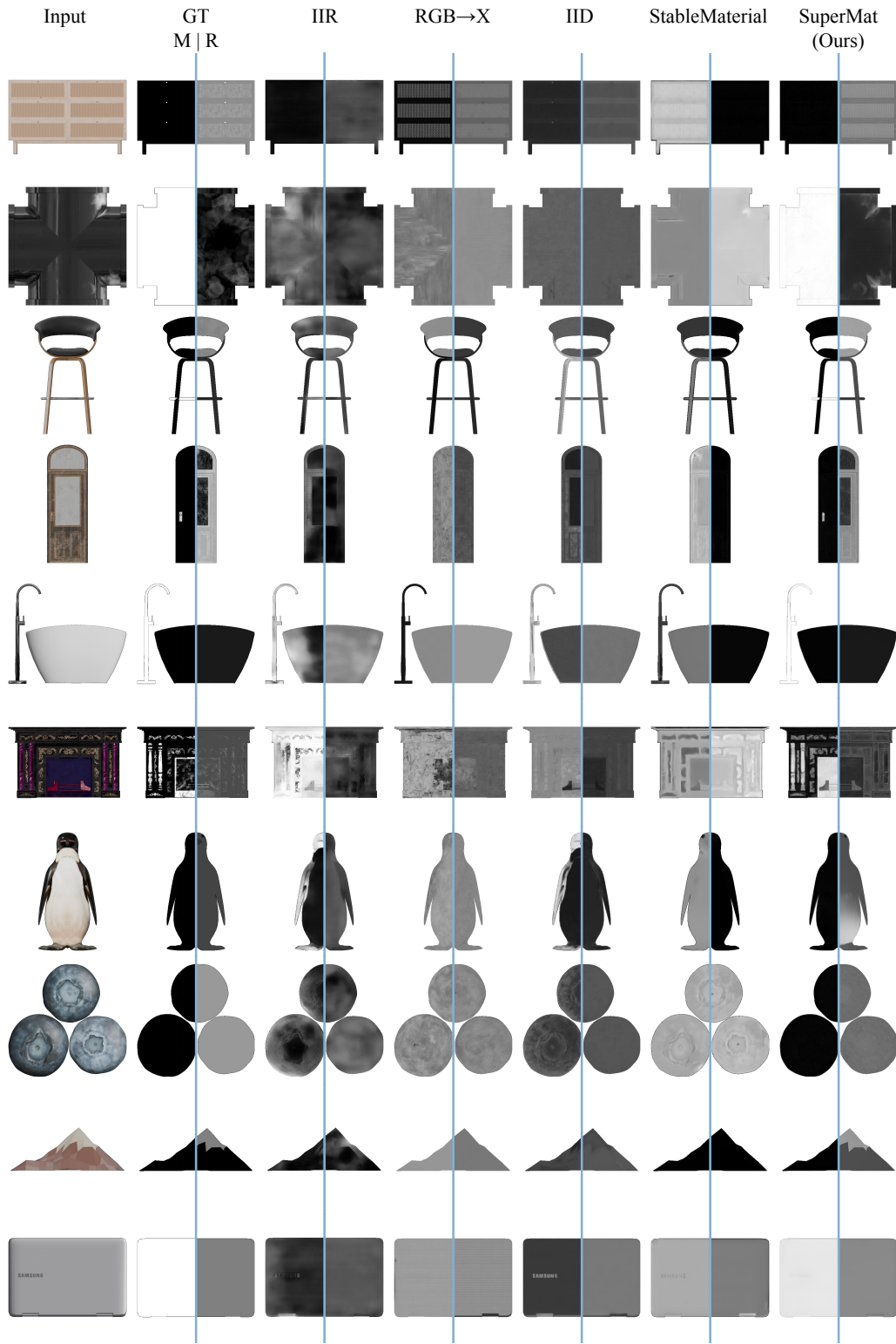


Figure 13. Additional metallic and roughness comparison from the BlenderVault test dataset. The metallic maps are shown on the left side (M), while the roughness maps are shown on the right side (R).

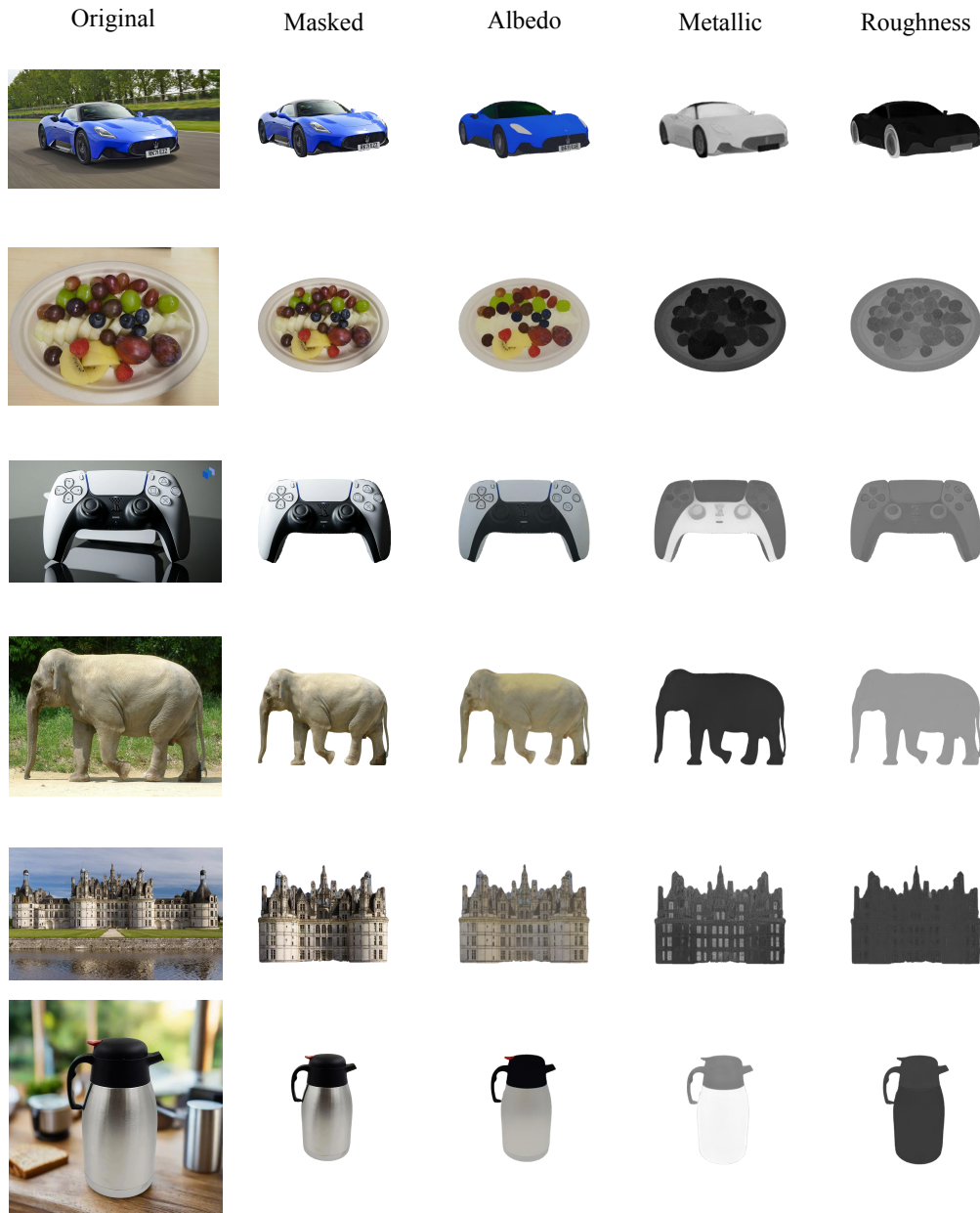


Figure 14. Additional results on real-world objects. The objects are extracted from captured images by SAM [19].

	Albedo			Metallic			Roughness			Relighting		
	PSNR \uparrow	SSIM \uparrow	LPIPS \downarrow	PSNR \uparrow	SSIM \uparrow	LPIPS \downarrow	PSNR \uparrow	SSIM \uparrow	LPIPS \downarrow	PSNR \uparrow	SSIM \uparrow	LPIPS \downarrow
L1	26.3745	0.9159	0.0987	21.8087	0.8733	0.2113	22.4262	0.9013	0.1308	25.8089	0.9300	0.0765
SSI	23.8053	0.9073	0.1067	21.6018	0.8378	0.2097	22.8090	0.9063	0.1261	23.8945	0.9242	0.0813
Perceptual	27.7214	0.9252	0.0771	23.1332	0.8799	0.1584	24.7161	0.9154	0.0926	28.0626	0.9424	0.0548

Table 2. Quantitative comparison across different loss functions. We highlight the **best** results for each metric.



Figure 15. Additional results of decomposition for 3D objects.

	Objaverse				BlenderVault			
	MSE↓	PSNR↑	SSIM↑	LPIPS↓	MSE↓	PSNR↑	SSIM↑	LPIPS↓
Derender3D	0.0094	22.0689	0.8529	0.1754	0.0104	22.4523	0.8919	0.1489
IIR	0.0130	21.3350	0.8705	0.1587	0.0202	20.5980	0.8654	0.1672
IID	0.0081	23.3557	0.8916	0.1212	0.0122	22.3877	0.8845	0.1395
RGB→X	0.0212	20.1405	0.8855	0.1362	0.0284	20.0958	0.8818	0.1452
IntrinsicAnything	0.0121	21.3502	0.8743	0.1481	0.0219	20.2352	0.8700	0.1682
StableMaterial	0.0101	23.8964	0.9038	0.0985	0.0143	23.9020	0.9061	0.1079
Ours w/o e2e	0.0058	24.9261	0.8997	0.0986	0.0102	24.3049	0.8935	0.1219
Ours w/o re-render	0.0023	27.7214	0.9252	0.0771	0.0043	26.7084	0.9185	0.0953
Ours	0.0020	28.1156	0.9284	0.0753	0.0044	26.8911	0.9195	0.0938

Table 3. Quantitative comparison on albedo. We highlight the best, second-best, and third-best results for each metric.

	Objaverse				BlenderVault			
	MSE↓	PSNR↑	SSIM↑	LPIPS↓	MSE↓	PSNR↑	SSIM↑	LPIPS↓
IIR	0.0471	16.1588	0.8401	0.1997	0.0515	17.6046	0.7835	0.2732
IID	0.0343	17.3157	0.8430	0.1954	0.0431	17.4303	0.7742	0.2866
RGB→X	0.0342	16.9451	0.8421	0.2127	0.0596	15.2457	0.7734	0.3149
StableMaterial	0.0391	17.2383	0.8481	0.2025	0.0839	14.7211	0.7775	0.3070
Ours w/o e2e	0.0353	18.7623	0.8696	0.1879	0.0470	20.9061	0.8455	0.2764
Ours w/o re-render	0.0134	23.1332	0.8799	0.1584	0.0330	22.7159	0.8150	0.2352
Ours	0.0125	23.5208	0.8845	0.1573	0.0291	23.3987	0.8351	0.2302

Table 4. Quantitative comparison on metallic. We highlight the best, second-best, and third-best results for each metric.

	Objaverse				BlenderVault			
	MSE↓	PSNR↑	SSIM↑	LPIPS↓	MSE↓	PSNR↑	SSIM↑	LPIPS↓
IIR	0.0195	20.7515	0.8877	0.1367	0.0334	19.1632	0.8621	0.1790
IID	0.0176	21.5627	0.8917	0.1174	0.0295	19.9655	0.8718	0.1586
RGB→X	0.0127	21.9641	0.8980	0.1190	0.0256	19.9961	0.8780	0.1561
StableMaterial	0.0261	19.4947	0.8872	0.1285	0.0587	17.0476	0.8197	0.2139
Ours w/o e2e	0.0161	21.1543	0.8858	0.1148	0.0278	20.4794	0.8679	0.1633
Ours w/o re-render	0.0070	24.7161	0.9154	0.0926	0.0221	21.9006	0.8933	0.1317
Ours	0.0070	24.7642	0.9144	0.0915	0.0214	22.2674	0.8935	0.1313

Table 5. Quantitative comparison on roughness. We highlight the best, second-best, and third-best results for each metric.

	Objaverse				BlenderVault			
	MSE↓	PSNR↑	SSIM↑	LPIPS↓	MSE↓	PSNR↑	SSIM↑	LPIPS↓
IIR	0.0124	22.5646	0.9021	0.1116	0.0296	20.4861	0.8782	0.1441
IID	0.0085	24.3354	0.9144	0.0903	0.0160	22.3058	0.9009	0.1142
RGB→X	0.0203	21.3419	0.9022	0.1007	0.0273	20.3137	0.8925	0.1231
StableMaterial	0.0131	23.1308	0.9082	0.0866	0.0263	21.2375	0.8866	0.1224
Ours w/o e2e	0.0072	25.5109	0.9219	0.0739	0.0171	23.1506	0.9031	0.1059
Ours w/o re-render	0.0041	28.0626	0.9424	0.0548	0.0123	25.5175	0.9259	0.0826
Ours	0.0035	28.4900	0.9465	0.0510	0.0106	25.7484	0.9266	0.0770

Table 6. Quantitative comparison on relighting. We highlight the best, second-best, and third-best results for each metric.